Integrative Omics Reveals Subtle Molecular Perturbations Following Ischemic Conditioning in a Porcine Kidney Transplant Model

Darragh P. O'Brien[1*], Adam M. Thorne[1,2*], Honglei Huang[1,2], Xuan Yao[1], Peter Søndergaard Thyrrestrup[3,4], Kristian Ravlo[3,5], Niels Secher[5,6], Rikke Norregaard[3,5], Rutger J. Ploeg[2], Bente Jespersen[3,5], Benedikt M. Kessler[1]

[1]Target Discovery Institute, Centre for Medicines Discovery, Nuffield Department of Medicine, University of Oxford, UK

[2]Nuffield Department of Surgical Sciences and Oxford Biomedical Research Centre, University of Oxford, UK

[3]Department of Renal Medicine, Aarhus University Hospital, Aarhus, Denmark

[4]Department of Anaesthesiology, Aalborg University Hospital, Aalborg Denmark

[5]Department of Clinical Medicine, Aarhus University, Aarhus, Denmark

[6]Department of Anaesthesiology and Intensive Care Medicine, Aarhus University Hospital, Aarhus Denmark

*these authors contributed equally

Corresponding authors:

darragh.obrien@ndm.ox.ac.uk; rutger.ploeg@nds.ox.ac.uk; bente.jespersen@clin.au.dk; benedikt.kessler@ndm.ox.ac.uk

Running Title:

Integrative Omic Profiling of a Porcine Kidney Transplant Model

ABSTRACT

Background: Remote Ischemic Conditioning (RIC) has been proposed as a therapeutic intervention to circumvent the Ischemia/reperfusion injury (IRI) that is inherent to organ transplantation. Using a porcine kidney transplant model, we aimed to decipher the subclinical molecular effects of a RIC regime, compared to non-RIC controls.

Methods: Kidney pairs (n = 8+8) were extracted from brain dead donor pigs and transplanted in juvenile recipient pigs following a period of cold ischemia. One of the two kidney recipients in each pair was subjected to RIC prior to kidney graft reperfusion, while the other served as non-RIC control. We designed an advanced integrative Omics strategy combining transcriptomics, proteomics, and phosphoproteomics to deduce molecular signatures in kidney tissue that could be attributed to RIC.

Results: In kidney grafts taken out 10 h after transplantation we detected minimal molecular perturbations following RIC compared to non-RIC at the transcriptome level, but more pronounced effects at the proteome level. In particular, we noted that RIC resulted in suppression of tissue inflammatory profiles. Furthermore, an accumulation of muscle extracellular matrix assembly proteins in kidney tissues was detected at the protein level, which may be in response to muscle tissue damage and/or fibrosis.

Conclusions: Our data identifies subtle molecular phenotypes in porcine kidneys following RIC and this knowledge could potentially aid optimisation of remote ischaemia protocols in renal transplantation.

Key Words:

Remote Ischemic Conditioning, Kidney Transplantation, Proteomics, Transcriptomics, Integrative Omics, Inflammation

BACKGROUND

Organ donation and transplantation inevitably involve periods of both warm and cold ischemia, as a consequence of diminished or restricted blood flow, which deprives the donor organ tissue of the oxygen required to maintain cellular metabolism. Subsequent reperfusion at time of implantation of the ischaemic graft results in tissue damage including several molecular hallmarks, such as hypoxic stress and production of reactive oxygen species, a rapid reduction of ATP levels, intracellular acidosis, and diminished nutritional supplies [1]. Combined, these insults lead to the activation of apoptotic and necrotic pathways, and if uncorrected, to graft fibrosis, organ dysfunction, and eventually rejection [2]. Acute kidney injury (AKI) induced by ischaemia and subsequent reperfusion is called delayed graft function in the clinical transplant setting and leads to the need of dialysis as well as a risk of poorer transplant outcome [3]. Remote ischaemic conditioning (RIC) has been proposed as a therapeutic modality to mitigate the effects of ischaemia/reperfusion injury (IRI) in organ transplantation [4, 5]. RIC is a simple procedure which involves short and repetitive cycles of non-damaging ischaemia, usually applied to a leg or arm, which may reduce damaging effects caused by IRI in the target organ. RIC has shown various outcomes in pre-clinical studies across different organs such as lung, liver, small intestine and in a variety of situations and species [6-11]. Several studies have demonstrated a reduction in IRI and improved early graft function in the recipient [12-15]. Regarding kidney transplantation and AKI, a protective effect of RIC in rodent renal models has been described, however the transition into the human setting has been challenging [14, 16]. Our previous work in a porcine model of kidney transplantation suggested a beneficial effect of RIC on early graft perfusion and function evidenced by a significantly improved renal plasma perfusion and glomerular filtration rate (GFR) [17]. When RIC was applied to kidney transplant patients in a clinical trial (CONTEXT), no clinical benefit was observed but this trial revealed distinct subclinical effects on kidney transplants at the molecular level [18]. In continuation of this, we revisited our RIC study carried out in pigs showing the potential positive effects of RIC that were actually the background for the CONTEXT study. Using samples obtained from our original porcine RIC model [17], we sought to identify possible proteomic

and transcriptomic changes in recipient tissue using advanced quantitative mass spectrometry and RNA sequencing. In this study, we describe altered molecular profiles comparable to the ones observed in human kidneys subjected to RIC.

METHODS

Transplant model

The effects of RIC versus non-RIC controls in porcine kidney transplants were evaluated in a paired randomised study, the design of which was described in detail by Soendergaard et al. [17]. Briefly, eight kidney pairs were taken from eight brain-dead donor pigs (60-64 kg) and transplanted into sixteen bilateral nephrectomised recipient pigs (14–16 kg), which were randomly given RIC or non-RIC within each pair. Prior to organ reperfusion, RIC was performed as indicated below. Pigs were surveyed, under anaesthesia, for 10 h after transplantation, assessing renal function by GFR, renal plasma perfusion and known renal biomarkers. The study was approved by the National Committee on Animal Research Ethics no. 2008-561-1584 (Animal Experiments Inspectorate, Copenhagen, Denmark) and conducted in accordance with the “Principles of Laboratory Animal Care” (NIH publication Vol. 25, No. 28 revised 1996).

Sample retrieval and ischemia regimen

Kidney retrieval, transplantation and RIC was performed by experienced transplant surgeons as described previously (**Figure 1**) [17]. Briefly, female Danish Landrace pigs were anaesthetised and placed under mechanical ventilation. Ringer's acetate was infused to maintain fluid balance and arterial pressure. Brain death was induced by increasing intracranial pressure. Kidneys were extracted, perfused and stored in 5°C cold storage solution. Two recipients were transplanted simultaneously after having their native kidneys removed. A RIC regimen was undertaken whereby the abdominal aorta was clamped above the aortic bifurcation but below the renal arteries in four cycles, with each

cycle consisting of 5 min of ischaemia and 5 min of reperfusion. Surgeons and investigators were unblinded to the treatment during the experiments. Renal biopsies from kidneys in the RIC and non-RIC groups were taken prior to termination after 10 hours reperfusion and snap frozen in liquid nitrogen for transcriptomic and proteomic analysis.

Transcriptomics analysis

Sample preparation. Sixteen tissue samples (weighing approximately 20 mg) were lysed using a Precellys 24 homogeniser (Bertin Instruments) in 350 µL of RNeasy Mini kit RLT lysis buffer. RNA was then extracted using RNeasy Mini kit (Qiagen, cat number: 74104) as per manufacturer's instructions. Purified RNA was eluted in 40 µL RNase-free H_2O and the approximate concentration evaluated using a NanoDrop ND-1000 spectrophotometer. Approximately, 450 ng of purified RNA was converted to cDNA by using high-capacity reverse transcription kit (Applied Biosystems, cat number: 4368814). For each reaction, a mix of 2 µL 10x RT buffer, 0.8 µL 25x dNPT mix, 2 µL 10x RT random primers, 1 µL Multiscribe reverse transcriptase, 3.2 µL nuclease free H_2O and 11 µL of RNA (40.9 ng/µL) was prepared. This was then primed at 25°C for 10 min, incubated at 37°C for 120 min and inactivated at 85°C for 5 min in a thermal cycler (VWR UNO 96). cDNA was then stored at -20°C until further use. An overview of the transcriptomics workflow is given in **Figure 1**.

For the analysis of the transcriptomics data described in this study, FASTQ files were converted to Binary-sequence Alignment Format (BAM) files using HISAT2 (v2.1.0) and Samtools (v1.3). Subsequently, BAM files were imported into Perseus software (v1.6.0.2) and genome annotation was performed using the Human Fasta cDNA database (http://www.ensembl.org). Reads per kilo per million (RPKM) values were calculated by a normalization step dividing by the sum (Normalization→Divide), followed by dividing normalized values by gene length, multiplying by 109, and taking the $\log_2$ values. The transcriptomics data set was deposited in ArrayExpress (AE) at EBI [19].

q-PCR. For q-PCR, primers for selected genes of interest were designed using Primer BLAST (see Table 1 for sequences), parameters included spanning exon-exon junctions, a target size of 200 bp and a maximum product size of 150. A Beta-Actin control gene was used as a reference [20]. A total of 20 µg of cDNA was used for each 20 µL reaction, in combination with 200 nM of each forward and reverse primer (Invitrogen) and Fast SYBR Green Master Mix (Applied Biosystems, cat number: 4385612), according to the manufacturer's instructions. The reaction plates were run on a Roche Lightcycler 480, with an initial pre-incubation of 37°C for 30 sec, then denaturing at 95°C for 3 sec, followed by annealing at 60°C for 30 sec. Denaturing and annealing was repeated for 40 runs before conducting melt curve analysis. Using Roche Lightcycler analysis software, the noise band was altered to exclude any background noise whilst staying within the lower third of the linear section of the curve to gain initial Ct values. Average Ct values for Beta-Actin were then subtracted from average Ct values of target genes to get dCt. RIC vs non-RIC groups and different time points were then compared using 2^-(x-y) to obtain relative expression levels and plotted on a box-dot graph.

Proteomics

Sample preparation. In accordance with the transcriptomics study, sixteen tissue samples (weighing approximately 20 mg) were lysed using a Precellys 24 homogeniser (Bertin Instruments) in 30 µL RIPA and 6M urea lysis buffer per 1 mg of tissue. Samples were reduced with 200 mM tris(2-carboxyethyl)phosphine (TCEP) at 55°C for 1 hour and alkylated with 375 mM iodoacetamide (IAA) for 30 min at room temperature. Following this, protein precipitation via methanol/chloroform precipitation was performed. The resulting pellet was dried and resuspended in 50 µL triethylammonium bicarbonate (TEAB) and the protein concentration determined using a BCA assay (Pierce). In total, 100 µg of protein was digested by trypsin using the SMART method (Thermo Scientific). In brief, each sample was loaded into a SMART digestion tube (Thermo Fisher Scientific, Cat no 60109-103) containing 150 µL of SMART digestion buffer. These were then incubated at 70°C at 1400 rpm for 2 hours on a heat shaker (Eppendorf) and spun at 2500 x g for 5 min, with collection of the supernatant. Samples were de-salted using SOLAµ SPE plates (Thermo Scientific, Cat no 60109-

103). Columns were equilibrated using 100% acetonitrile (ACN), then 0.1% trifluoroacetic acid (TFA). The samples were then diluted with 1% TFA and pulled through the column using a vacuum pump. They were then washed with 0.01% TFA and eluted in 100 µL 65% acetonitrile. Eluates were dried using a vacuum concentrator (SpeedVac, Thermo Scientific) and resuspended in 100 µL of 100 mM TEAB for Tandem Mass Tag (TMT) labelling.

TMT labelling and high pH fractionation. TMT 10plex reaction groups were used to label the digested peptides. Groups comprised of 8 samples (4 sets of RIC and non-RIC) and two pools; one undiluted, and one 5 times diluted. For labelling, 41 µL of TMT label was added to each sample and incubated for 1 hour at room temperature. To quench the reaction, 8 µL of 5% hydroxylamine was added to each sample and incubated at room temperature for 15 minutes. Equal volumes of each sample were then pooled into 2 groups, and de-salted using Sep-Pak C18 columns. The resulting eluent was dried using a vacuum concentrator (SpeedVac, Thermo Scientific) and resuspended in 120 µL of buffer A (98% MilliQ-H2O, 2% acetonitrile, 0.1% TFA). The two combined TMT 10plex experiments were then pre-fractionated using high pH 10.0 reversed-phase liquid chromatography (HPLC) into a total of 60 fractions. Fractions were subsequently concatenated into a total of 20 samples and submitted for LC-MS/MS analysis. The proteomic sample preparation strategy is summarized in **Figure 1**.

Phosphoproteomics. For phosphopeptide enrichment, 50 µg of protein was removed from each of the 16 tissue samples, and pooled into their respective RIC and non-RIC groups. Samples were reduced, alkylated, digested with trypsin, and desalted as above. Peptides (~400 µg) were eluted from Sep-Pak cartridges in 500 µL buffer B (65% ACN, 35% MilliQ-H2O, and 0.1% TFA). Phosphopeptide enrichment was performed using an Immobilized Metal Affinity Chromatography (IMAC) column with the aid of a Bravo Automated Liquid Handling Platform (Agilent).

Mass Spectrometry analysis. Liquid chromatography tandem mass spectrometry (LC–MS/MS) analysis was undertaken using a Dionex Ultimate 3000 nano-ultra reversed-phase HPLC system with on-line coupling to a Q Exactive High Field (HF) mass spectrometer (Thermo Scientific). Samples were

separated on an EASY-Spray PepMap RSLC C18 column (500 mm × 75 µm, 2 µm particle size; Thermo Fisher Scientific) over a 60 min gradient of 2–35% ACN in 5% dimethyl sulfoxide (DMSO), 0.1% FA, and the flow rate was ~ 250 nL/min. The mass spectrometer was operated in data-dependent analysis mode for automated switching between MS and MS/MS acquisition. Full MS survey scans were acquired from 400–2000 *m/z* at a resolution of 60,000 at 200 *m/z* and the top 12 most abundant precursor ions were selected for high collision energy dissociation fragmentation. MS2 fragment ion resolution was set to 15,000.

Data analysis. MS raw data files were searched using Proteome Discoverer (v2.3; total proteome) and MaxQuant (v1.5.14; phosphoproteome) software packages. Search parameters included the allowance of two missed trypsin cleavages. Carbamidomethylation (C) was set as a fixed modification, while TMT6plex (N-term, K), oxidation (M), deamidation (N, Q), and phosphorylation (STY) were set as variable modifications where appropriate. The data was searched against porcine protein sequences using the *UPR_Sus scrofa* fasta file along with the corresponding decoy reverse database. Only unique and razor peptides were used for quantitation.

Statistical analysis. TMT 10plex quantitation and data analysis was performed in Perseus software (v1.6.0.2) which filtered out contaminant and false positive identifications (decoys). The data were $\log_2$ transformed, and replicates were grouped into RIC and non-RIC. Missing values were imputed from the normal distribution and all samples were normalised by median subtraction. Hierarchical cluster analysis was performed on all the proteins identified by LC–MS/MS and visualised as heat maps using the Pearson correlation algorithm. Volcano plots were generated by applying parametric Student's t-tests between RIC and non-RIC controls, and using a Permutation FDR based correction for multiple testing. A Christmas tree plot was generated for the phosphoproteomics data where only one replicate was acquired. The mass spectrometry proteomics data have been deposited to the ProteomeXchange Consortium via the PRIDE [21] partner repository with the dataset identifier

195 PXD025273. Gene Ontology and biological pathway enrichment analysis was performed using STRING
196 protein–protein interaction networks & functional enrichment analysis (https://string-db.org/).

197

198 **RESULTS and DISCUSSION**

199 IRI is one of the primary causes of AKI during renal transplantation, and strategies to minimise it are
200 of urgent need [2]. Despite its early pre-clinical promise, the clinical utility of RIC has so far failed to
201 live up to expectations [16]. As a result, attention has shifted to the molecular profiling of organ tissues
202 in an attempt to decipher a more discreet subclinical response that may be triggered by RIC. Current
203 clinical parameters may not be refined enough to show nuances which, if enhanced, could result in
204 better outcomes. Using a cutting-edge integrative Omics strategy of transcriptomics, proteomics, and
205 phosphoproteomics, we sought to better understand the molecular and systemic footprint that is
206 inferred upon RIC in this porcine model of kidney transplantation.

207 We first performed RNA sequencing on kidney graft tissue to quantify changes at the transcriptome
208 level (**Figure 1**). A total of 19,220 transcripts were successfully quantified across RIC and non-RIC
209 groups (**Supplementary Table 1**). The majority of transcripts were found to be unchanged between
210 groups. Nevertheless, 33 transcripts had at least a two-fold change in abundance between groups, at
211 a *p*-value of ≤ 0.05 (**Figure 2, Supplementary Table 2**). The most notable of these included heat shock
212 protein beta-1 (HSPB1), monocarboxylate transporter 4 (SLC16A3), C-X-C motif chemokine (CXCL13),
213 C-C motif chemokine 2 (CCL2), interleukin-1 receptor type 2 (IL1R2), interleukin-1 beta (IL1B),
214 leukotriene B4 receptor 1 (LTB4R), Na(+)/H(+) exchange regulatory cofactor NHE-RF4 (PDZD3), and
215 Ras-like protein family member 10A (RASL10A), all of which were significantly down-regulated
216 following RIC. Moreover, biological pathway analysis revealed a reduction in the transcripts of genes
217 associated with regulation of inflammation following RIC as compared to their non-RIC counterparts
218 (**Figure 2, Supplementary Figure 1**). Transcript changes were confirmed by performing qPCR on a
219 selected panel of targets which were observed to be dysregulated in RIC in either our dataset, or as

described previously. We measured five genes in total in a pooled sample of each group, including IL1B, LTB4R, PDZD3, SLC16A3, and RASL10A (**Supplementary Table 3**). We observed a slight increase in RIC induced SLC16A3 transcripts, but overall, none of the genes quantified reached statistically significance between RIC and non-RIC, with all having a *p*-value of > 0.2 (**Figure 3**).

Following the analysis of the kidney donor biopsies at the transcriptome level, we extended the study to measure changes between the kidney tissue proteomes of the respective RIC and non-RIC groups. Our advanced quantitative proteomic strategy (**Figure 1**) successfully quantified a total of 7,546 proteins across all samples (**Supplementary Table 4**). Hierarchical clustering analysis revealed no clear discrimination between RIC and non-RIC groups at the proteome level (**Figure 2A**). Similarly, and in agreement with the transcriptomics results, the majority of proteins were found to be unchanged between groups. To determine if we could identify trends in the data, we took those proteins with the largest ($\geq \log_2 0.5$), albeit non-significant, fold changes forward for further analysis. In this context, 252 proteins were deemed to be differentially expressed between RIC and non-RIC groups (**Supplementary Table 5**). Mirroring the transcriptomics results, a dampening of immune response proteins was observed in RIC versus non-RIC tissue, whereby far the largest fold changes were observed in approximately 15 Ig-like domain-containing proteins (**highlighted in green in Figure 2B**). Attenuation of proteins involved in the inflammatory response associated with IRI could be one of the primary beneficial factors that could contribute to RIC renoprotection. This dampening may serve as a natural defence mechanism against the destruction caused by IRI. Despite this, the inflammatory response generally associated with renal transplantation, in the form of apoptotic cell death, macrophage and neutrophil infiltration, and anti-inflammatory cytokine production, was found to be unaffected by RIC in the pigs studied [22]. We performed pathway enrichment analysis on the differentially expressed proteins. Unfortunately, the Ig-like species described above could not be included due to lacking a mature porcine gene entry (**Supplementary Figure 2**). Mirroring the human CONTEXT study [18], there was an accumulation of muscle-derived and extracellular matrix assembly proteins in the renal tissue following RIC, including the collagens COL1A2, COL2A1, COL4A2, COL4A,

246 COL6A3, fibrillin and fibulin (**Figure 2, Supplementary Figure 2**), although no tourniquet on a limb but
247 rather clamping of the aorta was used in the present porcine study. Additionally, upregulation of
248 factors associated with innate immunity such as lysosome-associated membrane glycoprotein 1
249 (LAMP1), neutrophil cytosol factor 2 (NCF2), leucine-rich alpha-2-glycoprotein (LRG1),
250 myeloperoxidase (MPO), and properdin (CFP) were observed, suggesting the technique provoked the
251 activation of tissue remodelling cascades within the organ itself. Upregulation of these factors provide
252 a favourable environment for wound-healing and repair, and collagen scaffolds have been shown to
253 enhance survival of transplanted cardiomyoblasts and improve function in ischaemic rat hearts [23].
254 Increased collagen production has also been associated with a response to the hypoxic or anoxic
255 conditions inherent to surgery, ultimately leading to adhesion development [24]. It is, however,
256 unclear if these proteins provide a protective mechanism in RIC, or are a consequence of tissue
257 damage which could lead to fibrosis. Furthermore, we identified an up-regulation of several
258 components of the blood coagulation cascade, including Vitamin K-dependent protein C (PROC),
259 Fibrinogen beta chain (FGB), and Plasminogen (PLG). Interestingly, SLC16A3, IL1B, LTB4R, RASL10A,
260 and CXCL13, which were found to have some of the largest changes at the transcript level, were not
261 detected at the proteome level, while HSPB1, LTB4R, and PDZD3 transcripts were differentially
262 abundant, but found to be unchanged between non-RIC and RIC groups at the protein level.

263 To gain more insight into the signalling dynamics underlying these molecular changes in kidney tissue,
264 we performed phosphoproteomics to compare a global pool of all 8 RIC samples to that of the 8 non-
265 RIC controls. We identified 3,524 phosphosites across both groups, from a total of 3,626 proteins
266 **(Supplementary Table 6**). No substantial differences were identified in the phosphoproteome
267 between RIC and non-RIC groups, indicating little steady-state effects of RIC on kidney tissue at the
268 indicated time points (**Supplementary Figure 3**).

269 To determine if a joint analysis could reveal useful insights that could not be deciphered from
270 individual analysis alone, we integrated the transcriptomic and proteomic datasets (**Figure 4A**). Once

again, the Ig-like proteins that were found to be down-regulated in RIC in the proteomics dataset alone (**Figure 2B**) could not be included in this type of analysis due to a lack of matching cognate sequences at the transcriptome level. A low correlation was observed between the two datasets, with a Pearson correlation coefficient of 0.017. We subsequently performed 2D Annotation Enrichment Analysis in an effort to identify pathways which were simultaneously up- or down-regulated in both datasets [25]. Up-regulated pathways in RIC versus non-RIC and common to both datasets included muscle tissue development/remodelling, extracellular matrix disassembly, ubiquitin-specific protease activity, and steroid hormone receptor activity (**Figure 4**). Conversely, down-regulated pathways in RIC versus non-RIC and common to both included kidney development, vasodilation, epidermal growth factor receptor signalling, and the regulation of myoblast differentiation.

A possible explanation for the absence of significant proteomic and transcriptomic changes may be attributed to the condition of kidney tissue used in this study. The tissue had been through multiple insults, including brain death, periods of cold and warm ischemia and reperfusion. This makes it increasingly difficult to fully dissect the (perhaps comparatively minor) effect of RIC, despite a more aggressive RIC regimen than that in the human setting. A limiting factor of this study concerning Omics profiling is the low number of available samples, and the timepoint at which the analysed biopsies were taken. The end biopsies profiled for transcriptomics and proteomics were taken at termination after a 10-hour observation phase. Theoretically, this time period may be sufficient to induce a measurable change in gene expression, however it's possible that gene expression returns to that more similar to pre-RIC. Additionally, it may also be too early of a time point to measure a significant change in protein expression, which is possibly reflected in the lack of change identified at the proteomic depth achieved in this study. Ideally, there would be an observation phase of several days with multiple biopsies, however, this would require a survival model which was not feasible in combination with the severity of the RIC regimen.

CONCLUSIONS

In summary, RIC of the recipient before kidney graft reperfusion does not result in substantial molecular perturbations in the graft compared to non-RIC controls, which was confirmed by validation of selected candidates. The data did suggest, however, that the administered RIC caused tissue leakage and a potentially detrimental accumulation of muscle proteins in the kidney graft tissue, but also triggered an interplay between the innate and adaptive immune response, with a dampening of the latter. Ultimately however, our discovery studies showed no major differences in the transcriptomes and proteomes of porcine kidney transplant tissue following RIC, despite excellent depth of coverage in each.

LIST OF ABBREVIATIONS

AKI – Acute Kidney Injury

ATP – adenosine triphosphate

GFR – Glomerular Filtration Rate

IRI – Ischemic/Reperfusion Injury

RIC – Remote Ischemic Preconditioning

TMT – Tandem Mass Tag

DECLARATIONS

ETHICS APPROVAL AND CONSENT TO PARTICIPATE

Porcine kidney donor samples were taken from the porcine RIC study [17].

CONSENT FOR PUBLICATION

All authors have read the manuscript and given their consent for publication.

AVAILABILITY OF DATA AND MATERIALS

The mass spectrometry raw data files have been deposited under PRIDE Submission PXD025273. The transcriptomics data is available upon request to the authors.

COMPETING INTERESTS

The authors have no conflicts of interest to declare

FUNDING

Funding was provided by the Novo Nordisk Foundation, The Danish Medical Research Council, The Danish Kidney Association (Nyreforeningen), Department of Clinical Medicine, Aarhus University, Nuffield Department of Medicine, University of Oxford, and Nuffield Department of Surgical Sciences, University of Oxford.

AUTHORS CONTRIBUTIONS

DOB, AT, HH, XY, PS, KR and NS performed the experiments. BJ, RJP and BMK conceptualised the study. DOB, AT, BJ, RJP and BMK wrote the manuscript. DOB, AT, HH, LX, PS, KR and NS analysed the data. All authors read and approved the final manuscript.

ACKNOWLEDGEMENTS

The authors would like to thank members of the Kessler, Jespersen, and Ploeg research groups for helpful discussions and technical support.

AUTHORS' INFORMATION

Darragh P O'Brien and Adam M Thorne contributed equally to the work

340 ***Affiliations***

341 **Target Discovery Institute, Centre for Medicines Discovery, Nuffield Department of Medicine,**

342 **University of Oxford, UK**

343 Darragh P O'Brien, Adam M Thorne, Honglei Huang, Xuan Yao, Benedikt M Kessler

344 **Nuffield Department of Surgical Sciences and Oxford Biomedical Research Centre, University**

345 **of Oxford, UK**

346 Adam M Thorne, Honglei Huang, Rutger J Ploeg

347 **Department of Renal Medicine, Aarhus University Hospital, Aarhus, Denmark**

348 Bente Jespersen, Peter Søndergaard Thyrrestrup, Kristian Ravlo

349 Department of Anaesthesiology, Aalborg University Hospital, Aalborg Denmark

350 Peter Syndergaard Thyrrestrup

351 **Department of Clinical Medicine, Aarhus University, Aarhus, Denmark**

352 Rikke Norregaard, Bente Jespersen, Kristian Ravlo and Niels Secher

353 **Department of Anesthesiology and Intensive Care Medicine, Aarhus University Hospital, Aarhus**

354 **Denmark**

355 Niels Secher

356

357

358

359

360

361

FIGURE LEGENDS

Figure 1. ***Overview of transcriptomic and proteomic workflows***. **A**) For transcriptomics, tissue samples were cut, weight and lysed. RNA was extracted, followed by cDNA library preparation, and the difference in transcript level determined between non-RIC and RIC groups. For selected targets of interest, qPCR was undertaken. **B**) In the proteomics arm, proteins were extracted, reduced, alkylated and subjected to methanol/chloroform extraction, digested with trypsin, cleaned-up and subjected to 10plex TMT labelling. Labelled peptides were separated by high pH-RP, prior to analysis by LC-MS/MS. The green boxes outline our sample pooling and fractionation strategy. A total of 16 tissue samples (and 4 pools) were labelled across two TMT 10plex kits. Each TMT experiment was subsequently separated into 100 fractions, which were then concatenated down into 20 fractions. This resulted in a final total of 40 samples for injection into the mass spectrometer.

Figure 2. ***Transcriptome and proteome changes by RIC*** **A**) Hierarchical clustering analysis of RIC and non-RIC proteomes. **B**) Volcano plots displaying differential transcriptome expression on the left, and differential proteome expression on the right. The x-axis measures expression difference by log2(fold change), and the y-axis indicates statistical significance by $-\log_{10}(p\text{-value})$. Down-regulated species are coloured blue, while their up-regulated counterparts are coloured red. C) Enriched biological processes (Gene Ontology) determined from differentially-regulated transcripts and proteins (displayed by their gene symbol).

Figure 3. ***Minimal transcriptional alteration by RIC***. No statistically significant difference was observed for any of the selected qPCR targets (IL1B, LTB4R, PDZD3, SLC16A3, and RASL10A) between RIC and non-RIC groups, with all *p*-values > 0.2.

Figure 4. ***Integrated Omics reveals RIC induced tissue leakage and reduced inflammation***. A) Scatter plot of the *Log_2-fold-change* between RIC and non-RIC groups of the proteomics on the x-axis, versus the transcriptomics on the y-axis. Species which are down-regulated in both datasets are coloured blue, while their up-regulated counterparts are coloured red. A low Pearson correlation coefficient of

387 0.017 was observed. B) 2D Annotation Enrichment Analysis generated using transcripts and proteins
388 which were commonly dysregulated across the two datasets.

389

390 **Supplementary Figure S1.** ***Transcriptomic pathway enrichment analysis reveals subtle alteration of***
391 ***tissue inflammation by RIC***. All transcripts (n=33) which were found to be dysregulated in RIC versus
392 non-RIC controls were searched against the *Sus scrofa* database in STRING. Only interactions of the
393 highest confidence (scores > 0.90) were included in the analysis. Genes associated with immune
394 regulation are highlighted, with those linked to interleukin biology coloured red, while cytokines are
395 coloured purple.

396 **Supplementary Figure S2.** ***Proteomic pathway enrichment analysis uncovers RIC induced tissue***
397 ***leakage and altered inflammation***. Proteins (n=252) which were found to have the greatest
398 dysregulation in RIC versus non-RIC controls were searched against the *Sus scrofa* database in STRING.
399 Only interactions of the highest confidence (scores > 0.90) were included in the analysis.
400 Proteins/genes of interest are highlighted, with proteins associated with muscle and ECM coloured in
401 blue, blood coagulation in green, and factors associated with innate immunity coloured red.

402 **Supplementary Figure S3.** ***Kidney tissue phosphoproteomics unaffected by RIC***. A) Abundance plots
403 indicate no significant difference in the phosphoproteome between RIC and control groups. B) A
404 Christmas tree plot, with Significance B thresholds colour coded. Minor changes were observed
405 between groups.

406

407 **Table 1:** ***List of gene names and primer sequences used to conduct qPCR*****.** A total of five genes were
408 selected for qPCR validation of transcriptomics results, with beta actin serving as a control.

409 **Supplementary Table 1:** ***List of transcripts identified by transcriptomics*****.** A total of 19,220 transcripts
410 were successfully identified across groups.

Supplementary Table 2: ***Transcripts differentially expressed between RIC and Non-RIC groups*****.**

Supplementary Table 3: ***qPCR validation on a panel of targets from discovery transcriptomics.*** IL1B, LTB4R, PDZD3, SLC16A3, and RASL10A were quantified by qPCR. We observed a slight increase in RIC induced SLC16A3 transcripts, but overall, none of the genes quantified reached statistically significance between RIC and non-RIC, with all having a *p*-value of > 0.2

Supplementary Table 4: ***List of proteins identified by proteomics.*** A total of 7,546 proteins were successfully identified across groups.

Supplementary Table 5: ***Proteins differentially expressed between RIC and Non-RIC groups*****.**

Supplementary Table 6: ***List of proteins and phosphosites identified by phosphoproteomics.*** A total of 3,524 phosphosites were successfully identified across groups.

TABLES

Oligo Name	Forward Sequence (5' - 3')	Reverse Sequence (5' - 3')	Scale (µmole)
PDZD3	CCCTGTAAGTGCCCTGCTAT	CTCCAGGGATCAGAAGGATCG	0.025µmole
LTB4R	TGGTACTTCCTCTCTGGCTGA	CCATTGCAAGGACAGGCTTT	0.025µmole
RASL10A	TTGCATTTGGGGTAAACCTGGAA	GCCACTCCTCCAAGCTTAATTC	0.025µmole
SLC16A3	AGGTAACCTGAGACCTGGCT	TGGTTCCGCGTCCCTGG	0.025µmole
IL1B	CCAATTCAGGGACCCTACCC	GTTTTGGGTGCAGCACTTCAT	0.025µmole
Beta Actin	TGTCATGGACTCTGGGGATG	GGGCAGCTCGTAGCTCTTCT	0.025µmole

Table 1: List of gene names and primer sequences used to conduct qPCR. A total of five genes were selected for qPCR validation of transcriptomics results, with beta actin serving as a control.

REFERENCES

1. Wu, M.Y., et al., *Current Mechanistic Concepts in Ischemia and Reperfusion Injury.* Cell Physiol Biochem, 2018. **46**(4): p. 1650-1667.
2. Zhao, H., et al., *Ischemia-Reperfusion Injury Reduces Long Term Renal Graft Survival: Mechanism and Beyond.* EBioMedicine, 2018. **28**: p. 31-42.
3. Sharfuddin, A.A. and B.A. Molitoris, *Pathophysiology of ischemic acute kidney injury.* Nat Rev Nephrol, 2011. **7**(4): p. 189-200.
4. Zhou, D., et al., *Remote ischemic conditioning: a promising therapeutic intervention for multi-organ protection.* Aging (Albany NY), 2018. **10**(8): p. 1825-1855.
5. Thuret, R., et al., *Ischemic pre- and post-conditioning: current clinical applications.* Prog Urol, 2014. **24 Suppl 1**: p. S56-61.
6. Jiang, T., et al., *The Role of Remote Ischemic Preconditioning in Ischemia-Reperfusion Injury in Rabbits with Transplanted Lung.* Clin Lab, 2015. **61**(5-6): p. 481-6.
7. Vasdekis, S.N., et al., *The role of remote ischemic preconditioning in the treatment of atherosclerotic diseases.* Brain Behav, 2013. **3**(6): p. 606-16.
8. Vrakas, G., et al., *Synergistic Effect of Ischemic Preconditioning and Antithrombin in Ischemia-Reperfusion Injury.* Exp Clin Transplant, 2017. **15**(3): p. 320-328.
9. Magyar, Z., et al., *Beneficial effects of remote organ ischemic preconditioning on micro-rheological parameters during liver ischemia-reperfusion in the rat.* Clin Hemorheol Microcirc, 2018. **70**(2): p. 181-190.
10. Saeki, I., et al., *Ischemic preconditioning and remote ischemic preconditioning have protective effect against cold ischemia-reperfusion injury of rat small intestine.* Pediatr Surg Int, 2011. **27**(8): p. 857-62.
11. Qi, B., et al., *Effect of remote ischemic preconditioning among donors and recipients following pediatric liver transplantation: A randomized clinical trial.* World J Gastroenterol, 2021. **27**(4): p. 345-357.
12. Wu, G., et al., *Effect of remote ischemic preconditioning on hepatic ischemia-reperfusion injury in patients undergoing liver resection: a randomized controlled trial.* Minerva Anestesiol, 2020. **86**(3): p. 252-260.
13. Tuncer, F.B., et al., *Ischemic Preconditioning and Iloprost Reduces Ischemia-Reperfusion Injury in Jejunal Flaps: An Animal Model.* Plast Reconstr Surg, 2019. **144**(1): p. 124-133.
14. Jung, K.W., et al., *Effect of Remote Ischemic Preconditioning Conducted in Living Liver Donors on Postoperative Liver Function in Donors and Recipients Following Liver Transplantation: A Randomized Clinical Trial.* Ann Surg, 2020. **271**(4): p. 646-653.
15. Fuller, T.F., et al., *Ischemic preconditioning improves rat kidney graft function after severe ischemia/reperfusion injury.* Transplant Proc, 2005. **37**(1): p. 377-8.
16. Krogstrup, N.V., et al., *Remote Ischemic Conditioning on Recipients of Deceased Renal Transplants Does Not Improve Early Graft Function: A Multicenter Randomized, Controlled Clinical Trial.* Am J Transplant, 2017. **17**(4): p. 1042-1049.
17. Soendergaard, P., et al., *Improved GFR and renal plasma perfusion following remote ischaemic conditioning in a porcine kidney transplantation model.* Transpl Int, 2012. **25**(9): p. 1002-12.
18. Thorne, A.M., et al., *Subclinical effects of remote ischaemic conditioning in human kidney transplants revealed by quantitative proteomics.* Clin Proteomics, 2020. **17**(1): p. 39.
19. Athar, A., et al., *ArrayExpress update - from bulk to single-cell expression data.* Nucleic Acids Res, 2019. **47**(D1): p. D711-d715.
20. Li, Q., et al., *Evaluation of potential reference genes for relative quantification by RT-qPCR in different porcine tissues derived from feeding studies.* Int J Mol Sci, 2011. **12**(3): p. 1727-34.
21. Perez-Riverol, Y., et al., *The PRIDE database and related tools and resources in 2019: improving support for quantification data.* Nucleic Acids Res, 2019. **47**(D1): p. D442-d450.

22. Secher, N., et al., *No effect of remote ischaemic conditioning on inflammation in a porcine kidney transplantation model.* Transpl Immunol, 2014. **31**(2): p. 98-104.
23. Kutschka, I., et al., *Collagen matrices enhance survival of transplanted cardiomyoblasts and contribute to functional improvement of ischemic rat hearts.* Circulation, 2006. **114**(1 Suppl): p. I167-73.
24. Saed, G.M. and M.P. Diamond, *Hypoxia-induced irreversible up-regulation of type I collagen and transforming growth factor-beta1 in human peritoneal fibroblasts.* Fertil Steril, 2002. **78**(1): p. 144-7.
25. Cox, J. and M. Mann, *1D and 2D annotation enrichment: a statistical method integrating quantitative proteomics with complementary high-throughput data.* BMC Bioinformatics, 2012. **13 Suppl 16**(Suppl 16): p. S12.

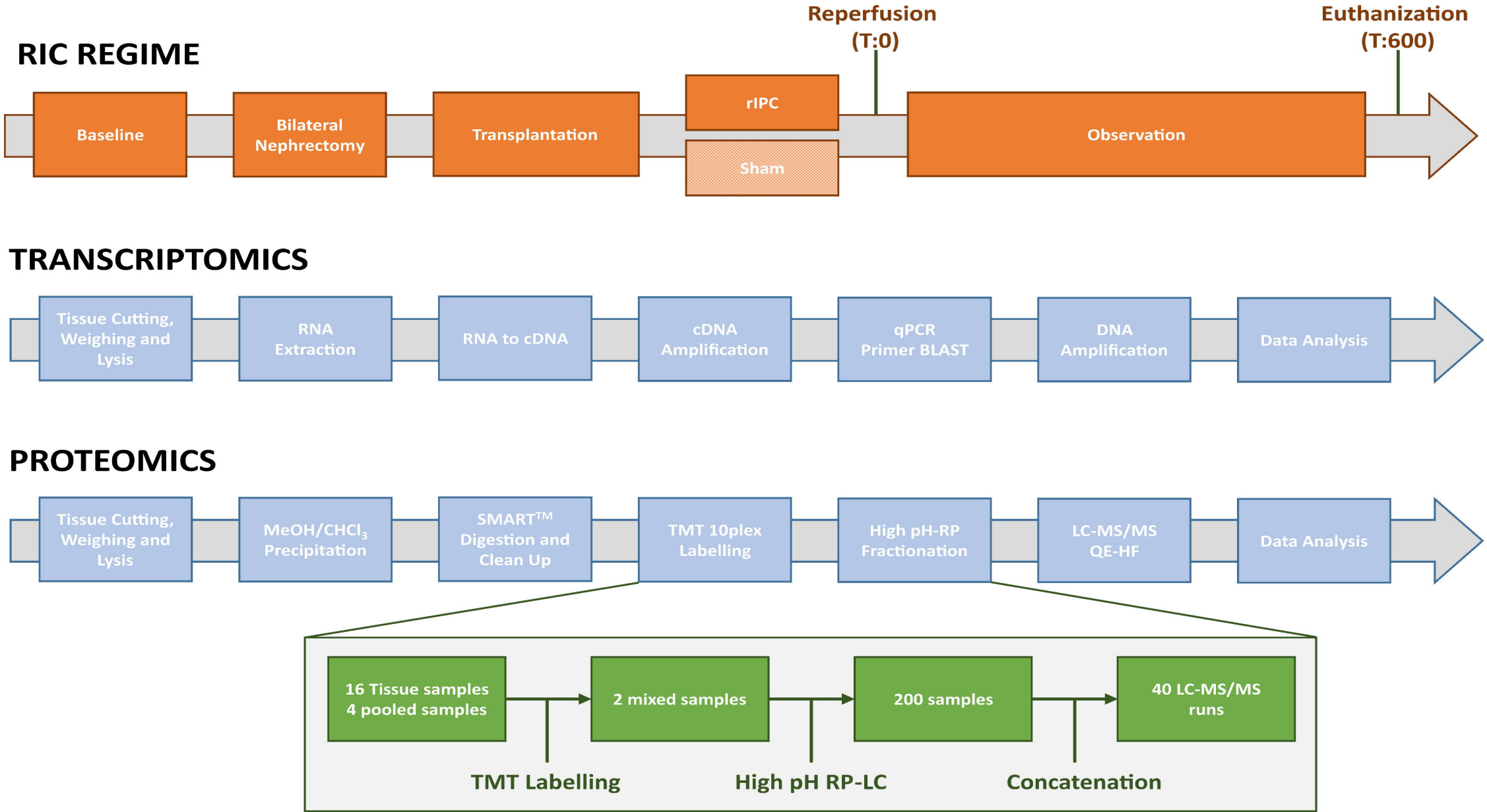
RIC REGIME
Reperfusion
(T:0)
Euthanization
(T:600)
Baseline
Bilateral
Nephrectomy
Transplantation
rIPC
Sham
Observation
TRANSCRIPTOMICS
Tissue Cutting,
Weighing and
Lysis
RNA
Extraction
RNA to cDNA
cDNA
Amplification
qPCR
Primer BLAST
DNA
Amplification
Data Analysis
PROTEOMICS
Tissue Cutting,
Weighing and
Lysis
MeOH/CHCl3
Precipitation
SMART™
Digestion and
Clean Up
TMT 10plex
Labelling
High pH-RP
Fractionation
LC-MS/MS
QE-HF
Data Analysis
16 Tissue samples
4 pooled samples
2 mixed samples
200 samples
40 LC-MS/MS
runs
TMT Labelling
High pH RP-LC
Concatenation

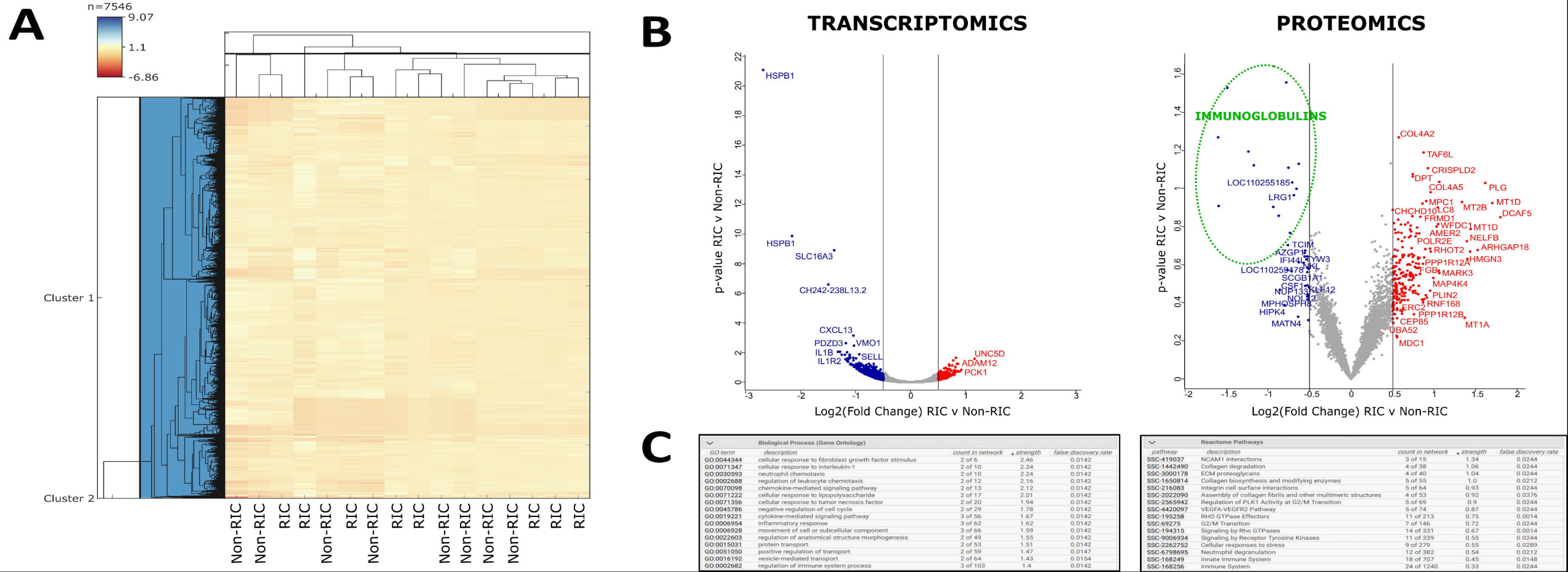
A
n=7546
9.07
1.1
-6.86
Cluster 1
Cluster 2
Non-RIC
Non-RIC
RIC
RIC
Non-RIC
RIC
Non-RIC
RIC
RIC
Non-RIC
Non-RIC
Non-RIC
Non-RIC
RIC
RIC
RIC
B
TRANSCRIPTOMICS
p-value RIC v Non-RIC
Log2(Fold Change) RIC v Non-RIC
HSPB1
HSPB1
SLC16A3
CH242-238L13.2
CXCL13
PDZD3
VMO1
IL1B
SELL
IL1R2
UNC5D
ADAM12
PCK1
PROTEOMICS
p-value RIC v Non-RIC
Log2(Fold Change) RIC v Non-RIC
IMMUNOGLOBULINS
LOC110255185
LRG1
TCIM
AZGP1
IFI44L
TYW3
LOC110259478
SCGB1A1
CSF1
NUP133
KLF12
NOL12
MPHOSPH8
HIPK4
MATN4
COL4A2
TAF6L
CRISPLD2
DPT
COL4A5
PLG
MPC1
MT2B
MT1D
CHCHD10
LC8
DCAF5
FRMD1
WFDC1
MT1D
AMER2
POLR2E
NELFB
RHOT2
ARHGAP18
PPP1R12A
HMGN3
FGB
MARK3
MAP4K4
PLIN2
RNF168
ERC2
PPP1R12B
CEP85
MT1A
UBA52
MDC1
C
Biological Process (Gene Ontology)
GO-term | description | count in network | strength | false discovery rate
GO:0044344 | cellular response to fibroblast growth factor stimulus | 2 of 6 | 2.46 | 0.0142
GO:0071347 | cellular response to interleukin-1 | 2 of 10 | 2.24 | 0.0142
GO:0030593 | neutrophil chemotaxis | 2 of 10 | 2.24 | 0.0142
GO:0002688 | regulation of leukocyte chemotaxis | 2 of 12 | 2.16 | 0.0142
GO:0070098 | chemokine-mediated signaling pathway | 2 of 13 | 2.12 | 0.0142
GO:0071222 | cellular response to lipopolysaccharide | 2 of 17 | 2.01 | 0.0142
GO:0071356 | cellular response to tumor necrosis factor | 2 of 20 | 1.94 | 0.0142
GO:0045786 | negative regulation of cell cycle | 2 of 29 | 1.78 | 0.0142
GO:0019221 | cytokine-mediated signaling pathway | 3 of 56 | 1.67 | 0.0142
GO:0006954 | inflammatory response | 3 of 62 | 1.62 | 0.0142
GO:0006928 | movement of cell or subcellular component | 3 of 66 | 1.59 | 0.0142
GO:0022603 | regulation of anatomical structure morphogenesis | 2 of 49 | 1.55 | 0.0142
GO:0015031 | protein transport | 2 of 53 | 1.51 | 0.0142
GO:0051050 | positive regulation of transport | 2 of 59 | 1.47 | 0.0147
GO:0016192 | vesicle-mediated transport | 2 of 64 | 1.43 | 0.0154
GO:0002682 | regulation of immune system process | 3 of 103 | 1.4 | 0.0142
Reactome Pathways
pathway | description | count in network | strength | false discovery rate
SSC-419037 | NCAM1 interactions | 3 of 15 | 1.34 | 0.0244
SSC-1442490 | Collagen degradation | 4 of 38 | 1.06 | 0.0244
SSC-3000178 | ECM proteoglycans | 4 of 40 | 1.04 | 0.0244
SSC-1650814 | Collagen biosynthesis and modifying enzymes | 5 of 55 | 1.0 | 0.0212
SSC-216083 | Integrin cell surface interactions | 5 of 64 | 0.93 | 0.0244
SSC-2022090 | Assembly of collagen fibrils and other multimeric structures | 4 of 53 | 0.92 | 0.0376
SSC-2565942 | Regulation of PLK1 Activity at G2/M Transition | 5 of 69 | 0.9 | 0.0244
SSC-4420097 | VEGFA-VEGFR2 Pathway | 5 of 74 | 0.87 | 0.0244
SSC-195258 | RHO GTPase Effectors | 11 of 213 | 0.75 | 0.0014
SSC-69275 | G2/M Transition | 7 of 146 | 0.72 | 0.0244
SSC-194315 | Signaling by Rho GTPases | 14 of 331 | 0.67 | 0.0014
SSC-9006934 | Signaling by Receptor Tyrosine Kinases | 11 of 339 | 0.55 | 0.0244
SSC-2262752 | Cellular responses to stress | 9 of 279 | 0.55 | 0.0289
SSC-6798695 | Neutrophil degranulation | 12 of 382 | 0.54 | 0.0212
SSC-168249 | Innate Immune System | 18 of 707 | 0.45 | 0.0148
SSC-168256 | Immune System | 24 of 1240 | 0.33 | 0.0244

IL1B

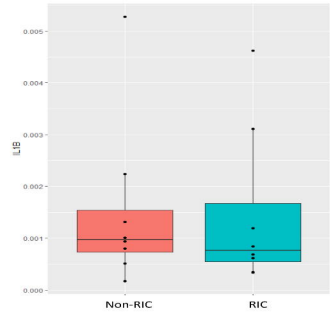

LTB4R

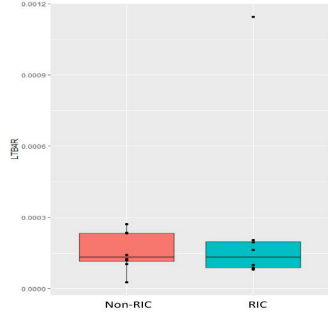

PDZD3

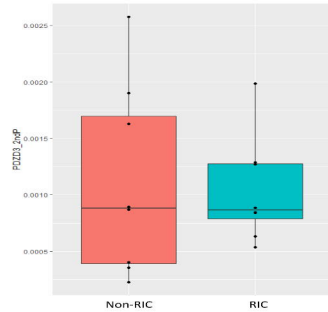

SLC16A3

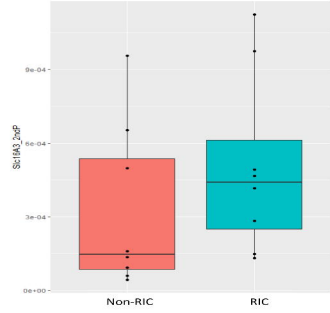

RASL10A

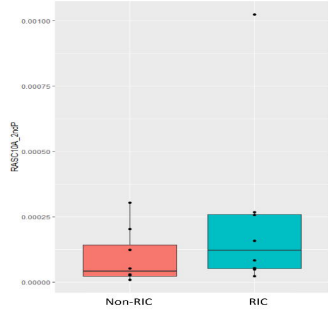

Gene	*p*-value (RIC v Non-RIC)
IL1B	0.942122575
LTB4R	0.414858107
PDZD3	0.842717016
SLC16A3	0.207829143
RASL10A	0.284549205

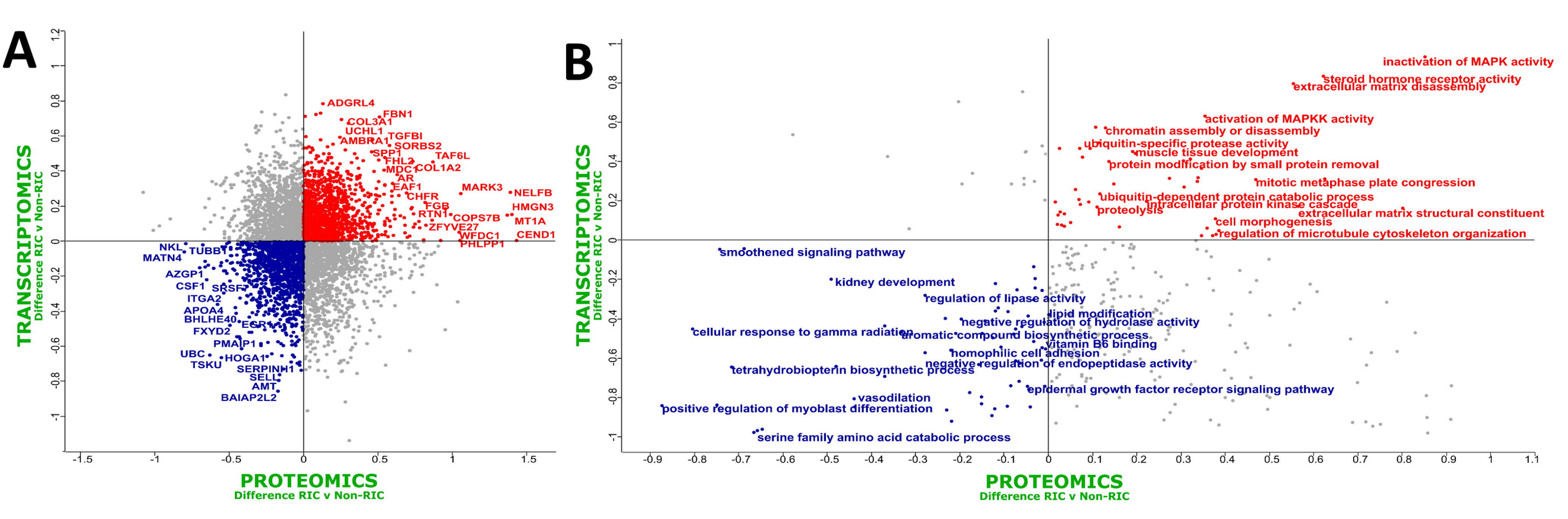
A
TRANSCRIPTOMICS
Difference RIC v Non-RIC
PROTEOMICS
Difference RIC v Non-RIC
ADGRL4
FBN1
COL3A1
UCHL1
TGFBI
AMBRA1
SORBS2
SPP1
TAF6L
FHL2
MDC1
COL1A2
AR
EAF1
MARK3
NELFB
CHFR
HMGN3
FGB
RTN1
COPS7B
MT1A
ZFYVE27
CEND1
WFDC1
PHLPP1
NKL
TUBB
MATN4
AZGP1
CSF1
SRSF7
ITGA2
APOA4
BHLHE40
EGR1
FXYD2
PMAIP1
UBC
HOGA1
TSKU
SERPINH1
SELL
AMT
BAIAP2L2
B
TRANSCRIPTOMICS
Difference RIC v Non-RIC
PROTEOMICS
Difference RIC v Non-RIC
inactivation of MAPK activity
steroid hormone receptor activity
extracellular matrix disassembly
activation of MAPKK activity
chromatin assembly or disassembly
ubiquitin-specific protease activity
muscle tissue development
protein modification by small protein removal
mitotic metaphase plate congression
ubiquitin-dependent protein catabolic process
intracellular protein kinase cascade
proteolysis
extracellular matrix structural constituent
cell morphogenesis
regulation of microtubule cytoskeleton organization
smoothened signaling pathway
kidney development
regulation of lipase activity
lipid modification
negative regulation of hydrolase activity
cellular response to gamma radiation
aromatic compound biosynthetic process
vitamin B6 binding
homophilic cell adhesion
negative regulation of endopeptidase activity
tetrahydrobiopterin biosynthetic process
epidermal growth factor receptor signaling pathway
vasodilation
positive regulation of myoblast differentiation
serine family amino acid catabolic process